

UDFT and MCSCF Descriptions of the Photochemical Bergman Cyclization of Enediynes

Aurora E. Clark, Ernest R. Davidson,* and Jeffrey M. Zaleski*

Contribution from the Department of Chemistry, Indiana University, Bloomington, Indiana 47405-7102

Received November 17, 2000

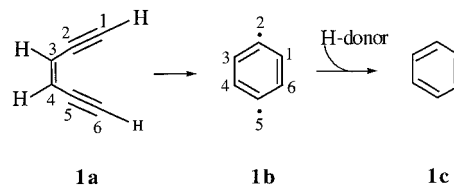
Abstract: Several singlet and triplet potential energy surfaces (PES) for the Bergman cyclization of *cis*-1,5-hexadiyne-3-ene (**1a**) have been computed by UDFT, CI, CASCI, CASSCF, and CASMP2 methods. It is found that the first six excited states of **1a** can be qualitatively described as linear combinations of the configurations of weakly interacting ethylene and acetylene units. Although the symmetry relaxation from C_{2v} to C_2 makes cyclization of the 1^3B state Woodward–Hoffmann allowed, it also increases the probability of competing *cis*–*trans* isomerization. Hydrogen atom abstraction is another plausible pathway because the terminal alkyne carbons possess a large radical character. In view of the competing processes, we conclude that the Bergman cyclization along the 1^3B path is unlikely despite its exothermicity ($\Delta H_{\text{rxn}}^{\text{CASMP2}} = -42$ kcal/mol). Calculations on cyclic analogues of **1a** lead to similar conclusions. A less exothermic, but more plausible pathway for photochemical cyclization lies on the 2^1A PES ($\Delta H_{\text{rxn}}^{\text{CASMP2}} = -18$ kcal/mol). Compared to the 1^1A_1 and 1^3B states, the 2^1A state has less in-plane electron repulsion which may facilitate cyclization. The resulting *p*-benzynes intermediate has an unusual electronic structure combining singlet carbene and open-shell diradical features. Deactivation of the 2^1A state of **1a** is a competing pathway.

Introduction

Bergman cyclization, epitomized by the 1,6-intramolecular rearrangement of *cis*-1,5-hexadiyne-3-ene (**1a**) into the 1,4-phenyl diradical (**1b**), is one of the most intriguing unimolecular reactions in chemistry (Scheme 1).

The process may be induced both thermally^{1–8} and photochemically^{9–12} to produce the intermediate **1b** which is responsible for the observed H-atom abstraction from organic substrates.^{13,14} Interest in enediyne chemistry has burgeoned following the discovery of naturally occurring molecules that contain the 1,5-diyne-3-ene moiety and cleave DNA with the toxic diradical intermediate **1b**.^{15–17} A great deal of theoretical and experi-

Scheme 1



mental effort has afforded a fairly good understanding of the thermally induced Bergman reaction of simple enediynes.¹⁸ In contrast, the mechanism of the photochemical cyclization is not yet understood.

The first photochemically induced Bergman cyclization was observed by Campbell in 1968.¹⁹ The reaction did not attract much attention until 1993 when acyclic enediynes were shown to undergo *cis*–*trans* isomerization and cleave DNA in the presence of a photosensitizing agent.¹² In 1994, Turro and co-workers reported the photosensitized Bergman cyclization of a phenyl-substituted enediyne, presumably proceeding through a 1,4-dehydronaphthalene intermediate analogous to that expected in the corresponding thermal rearrangement.⁹ In 1996, Funk et al. made similar observations while studying photochemically

* To whom correspondence should be addressed. E-mail: davidson@indiana.edu. E-mail: zaleski@indiana.edu.

(1) Nicolaou, K. C.; Zuccarello, G.; Ogawa, Y.; Schweiger, E. J.; Kumazawa, T. *J. Am. Chem. Soc.* **1988**, *110*, 4866.

(2) Nicolaou, K. C.; Ogawa, Y.; Zuccarello, G.; Kataoka, H. *J. Am. Chem. Soc.* **1988**, *110*, 7247.

(3) Magnus, P.; Carter, P. A. *J. Am. Chem. Soc.* **1988**, *110*, 1626.

(4) Russell, K. C.; Kim, C. *J. Org. Chem.* **1998**, *63*, 8229.

(5) König, B.; Pitsch, W. *J. Org. Chem.* **1996**, *61*, 4258.

(6) Nicolaou, K. C.; Maligres, P.; Shin, J.; De Leon, E.; Rideout, D. J. *Am. Chem. Soc.* **1990**, *112*, 7825.

(7) Semmelhack, M. F.; Neu, T.; Foubelo, F. *Tetrahedron Lett.* **1992**, *33*, 3277.

(8) Bergman, R. G.; Jones, R. R. *J. Am. Chem. Soc.* **1972**, *94*, 660.

(9) Turro, N. J.; Evenzahav, A.; Nicolaou, K. C. *Tetrahedron Lett.* **1994**, *35*, 8089.

(10) Turro, N.; Evenzahav, A. *J. Am. Chem. Soc.* **1998**, *120*, 1835.

(11) Funk, R. L.; Young, E. R. R.; Williams, R. M.; Flanagan, M. F. *J. Am. Chem. Soc.* **1996**, *118*, 3291.

(12) Kagen, J.; Wang, X.; Chen, X.; Lau, K. Y.; Batac, I. V.; Tuveson, R. W.; Hudson, J. B. *J. Photochem. Photobiol., B* **1993**, *21*, 135.

(13) Bergman, R. G.; Comita, P. B.; Lockhart, T. P. *J. Am. Chem. Soc.* **1981**, *103*, 4082.

(14) Marquardt, R.; Balster, A.; Sander, W.; Kraka, E.; Cremer, D.; Radziszewski, J. G. *Angew. Chem., Int. Ed.* **1998**, *110*, 1001.

(15) Smith, A. L.; Nicolaou, K. C. *J. Med. Chem.* **1996**, *39*, 2103.

(16) Kaneko, T.; Takahashi, M.; Hiram, M. *Tetrahedron Lett.* **1999**, *40*, 2015.

(17) Konishi, M. *Antibiot.* **1989**, *42*, 1449.

(18) (a) Grissom, J. W.; Gunawardena, G. U.; Klingberg, D.; Huang, D. *Tetrahedron* **1996**, *52*, 6453. (b) Squires, R. R.; Nash, J. J.; Wierschke, S. G. *J. Am. Chem. Soc.* **1993**, *115*, 11958. (c) Kraka, E.; Cremer, D. *J. Am. Chem. Soc.* **1994**, *116*, 4929. (d) Chen, P.; Logan, C. F. *J. Am. Chem. Soc.* **1996**, *118*, 2113. (e) Morokuma, K.; Koga, N. *J. Am. Chem. Soc.* **1991**, *113*, 1907. (f) Cramer, C. J.; Squires, R. R.; Nash, J. J. *Chem. Phys. Lett.* **1997**, *277*, 311. (g) Schreiner, P. R.; Shaik, S.; Wittkopp, A.; Galbraith, J. M.; Harris, N.; Wei, W. *Chem. Eur. J.* **2000**, *6*, 1446. (h) Schreiner, P. R. *J. Am. Chem. Soc.* **1998**, *120*, 4184. (i) Lindh, R.; Bernhardtsson, A.; Schütz, M. *J. Phys. Chem. A* **1999**, *103*, 9913. (j) Lindh, R.; Persson, B. J. *J. Am. Chem. Soc.* **1994**, *116*, 4963. (k) Koseki, S.; Hiram, M.; Fujimura, Y. *J. Phys. Chem. A* **1999**, *103*, 7672. (l) Yu, C.; Chang, N.; Chen, W. *J. Phys. Chem. A* **1998**, *102*, 2584.

(19) Campbell, I. D.; Eglington, G. J. *Chem. Soc. C* **1968**, 2120.

induced DNA cleavage by water soluble analogues of enediynes.¹¹ More recently, Turro et al. established that the photo-Bergman product, along with other photoreduction products can be obtained by *direct* excitation of the enediyne moiety.¹⁰ Product distributions and yields were determined to depend on the substituents at the alkyne termini. Furthermore, triplet sensitization studies showed that the photo-Bergman product may result from either singlet or triplet excited electronic states of the enediyne, while photoreduction products derive solely from the photoinduced excited triplet population. These findings were rationalized in terms of variations in intersystem crossing (ISC) efficiencies between the enediyne analogues.

Although detailed product analyses indicate that photoinduced Bergman cyclization is indeed possible, the available mechanistic information is not sufficient to construct a predictive model. To our knowledge, no theoretical studies of the photochemical Bergman cyclization have been performed to date. In this paper we report the results of calculations of the ground state (S_0) and lowest-energy triplet (T_1) PES for the cyclization of **1a** into **1b**, as well as optimizations of the S_1 structures of **1a** and **1b**. The reactivity of enediynes is studied by following the electronic structure and orbital symmetries from the reactant **1a** to the diradical intermediate **1b** along these PES. The results indicate the possibility of photochemically initiated Bergman cyclization along an excited singlet PES with deactivation of the S_1 state of **1a** as a competing pathway.

Computational Methods

Geometry optimizations of S_0 and T_1 states were performed by the (U)B3LYP and (U)BPW91 methods using the Gaussian 98²⁰ program, and by the complete active space self-consistent field (CASSCF) method for S_0 , T_1 , and S_1 states using HONDO 99.²¹ As noted by Gräfenstein, a spin-unrestricted density functional theory (UDFT) calculation for closed-shell species such as the ground state **1a** and the transition state (TS) **1[‡]** produces the same results as restricted density functional theory (RDFT).²² However, when describing the singlet diradical intermediate **1b**, RDFT becomes unstable with respect to spin-symmetry breaking, and a lower-energy UDFT solution usually exists. To ensure the lowest-energy solution, we used UDFT in all instances. The 6-31G* basis set was employed in all density functional theory (DFT) calculations, while the CASSCF calculations utilized a similar basis with 5-component d functions. Since the symmetries of the optimal structures were initially unknown, we started the optimizations with C_1 geometries. Optimization of the S_0 , T_1 , and S_1 states along the reaction path resulted in structures of C_{2v} , C_2 , and C_1 symmetries, respectively.

For the C_{2v} structures (assuming the molecule is in the yz plane), the CAS was generated by distributing 10 electrons among 10 orbitals including the two in-plane ($\pi_{||}$) orbitals ($9a_1, 8b_2$), the three out-of-plane (π_{\perp}) orbitals ($1b_1, 1a_2, 2b_1$), and the five corresponding virtual orbitals ($2a_2, 10a_1, 9b_2, 3b_1, 3a_2$) of the enediyne moiety. The two $\pi_{||}$ orbitals travel along the reaction coordinate into the a_1 σ -orbital of the new C–C bond and the b_2 σ -orbital localized on the radical centers. A second-order Møller–Plesset perturbation theory (MP2) calculation with

Table 1. Interatomic Distances (Å) and Bond Angles (deg) for the Singlet Ground State of **1a**, the Corresponding TS, and Diradical **1b** Computed with Various Methods and the 6-31G* Basis Set

system	method	r_{25}	r_{16}	r_{32}	r_{34}	r_{21}	α_{21H}	α_{321}^a	α_{432}
1a	expt. ^b		4.320	1.429	1.347	1.208	179.4	181.2	123.9
	CASSCF	3.003	4.488	1.434	1.350	1.211	178.6	182.6	125.2
	UB3LYP	2.997	4.481	1.417	1.355	1.211	178.7	182.4	125.4
	UBPW91	3.017	4.538	1.415	1.368	1.223	178.3	182.8	125.6
1[‡]	CASSCF	2.782	1.917	1.419	1.381	1.283	140.8	130.7	119.6
	UB3LYP	2.742	1.982	1.395	1.402	1.265	147.8	133.8	118.7
	UBPW91	2.761	2.124	1.410	1.407	1.267	150.9	136.6	118.9
	CASSCF	2.719	1.442	1.377	1.412	1.382	121.8	124.2	117.6
1b	UB3LYP	2.686	1.422	1.374	1.422	1.374	123.0	125.4	117.3
	UBPW91	2.706	1.436	1.377	1.436	1.377	123.6	125.1	117.5

^a The angle $\alpha_{321} = \alpha_{456}$ is defined in Figure 1. ^b See ref 27.

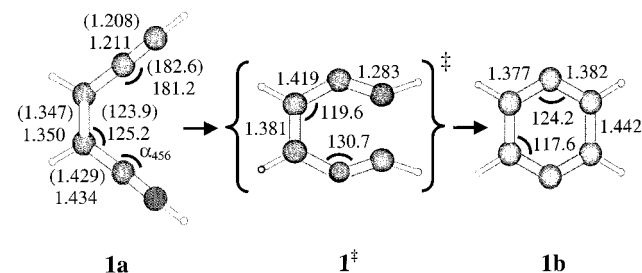


Figure 1. 10 e[−]/10 orbital CASSCF/6-31G* optimized structures along the 1A_1 (S_0) PES for the Bergman cyclization of **1a**.

the CASSCF reference wave function (CASMP2) was performed at the optimized CASSCF geometry to obtain a more accurate energy. Because of CASMP2 program limitations,²³ the calculation could only be performed with eight active electrons, so that the 8 e[−]/8 orbital CAS reference was obtained from the 10 e[−]/10 orbital CAS by excluding the most occupied and least occupied orbitals at each point along the PES. The multireference singles and doubles CI (MRSDCI) method was employed to test the CASSCF wave functions for relevant configurations outside of the active space. Configurations that contributed more than 99% to the CASSCF wave function were used as the MRSDCI reference configurations. Both the MRSDCI and the density of effectively unpaired electrons²⁴ $D(r)$ (which is identical with the density of odd electrons described by Takatsuka et al.²⁵) were computed with the MELD²⁶ suite of programs. Two types of $D(r)$ plots were generated. The in-plane density of planar structures was plotted by taking the in-plane section of $D(r)$. All other density plots (labeled morphed density plots) were generated by dropping the centers of the basis functions into the plotting plane while keeping the original MO coefficients.

The properties of the first six vertical excited states of **1a** were determined by three methods: (a) full CI within the 10 e[−]/10 orbital CAS (referred to as CASCI), (b) CASSCF, and (c) CASMP2 with the 8 e[−]/8 orbital CAS reference. All methods used the optimized 10 e[−]/10 orbital S_0 orbitals as the initial guess.

Ground-State PES (1A_1)

Geometry and Electronic Structure. Both DFT and CASSCF methods accurately reproduce the experimental geometry of **1a** (Table 1, Figure 1). UBPW91 tends to overestimate bond lengths and angles relative to CASSCF and UB3LYP structures. The CASSCF wave function is dominated by a single configuration $|\dots 8b_2^2\rangle$. In the CASSCF structure of **1a**, the bond

(20) Frisch, M. J.; Trucks, G. W.; Schlegel, H. B.; Scuseria, G. E.; Robb, M. A.; Cheeseman, J. R.; Zakrzewski, V. G.; Montgomery, J. A., Jr.; Stratmann, R. E.; Burant, J. C.; Dapprich, S.; Millam, J. M.; Daniels, A. D.; Kudin, K. N.; Strain, M. C.; Farkas, O.; Tomasi, J.; Barone, V.; Cossi, M.; Cammi, R.; Mennucci, B.; Pomelli, C.; Adamo, C.; Clifford, S.; Ochterski, J.; Petersson, G. A.; Ayala, P. Y.; Cui, Q.; Morokuma, K.; Malick, D. K.; Rabuck, A. D.; Raghavachari, K.; Foresman, J. B.; Cioslowski, J.; Ortiz, J. V.; Baboul, A. G.; Stefanov, B. B.; Liu, G.; Laishenko, A.; Piskorz, P.; Komaromi, I.; Gomperts, R.; Martin, R. L.; Fox, D. J.; Keith, T.; Al-Laham, M. A.; Peng, C. Y.; Nanayakkara, A.; Gonzalez, C.; Challacombe, M.; Gill, P. M. W.; Head-Gordon, M.; Replogle, E. S.; Pople, J. A. *Gaussian 98*, version A.6; Gaussian Inc.: Pittsburgh, PA, 1998.

(21) Dupuis, M.; Marquez, A.; Davidson, E. R. *HONDO 99.6*; IBM Corporation: Kingston, NY, 1999.

(22) Gräfenstein, J.; Hjerpe, A. M.; Kraka, E.; Cremer, D. *J. Phys. Chem. A* **2000**, *104*, 1748.

(23) Kozłowski, P. M.; Davidson, E. R. *J. Chem. Phys.* **1994**, *100*, 3672.

(24) Davidson, E. R.; Staroverov, V. N. *J. Am. Chem. Soc.* **2000**, *122*, 186.

(25) Takatsuka, K.; Fueno, T.; Yamaguchi, K. *Theor. Chim. Acta* **1978**, *48*, 175.

(26) MELD is a set of electronic structure programs written by L. E. McMurchie, S. T. Elbert, S. R. Langhoff, and E. R. Davidson, with extensive modifications by D. Feller and D. C. Rawlings. Available from <http://php.indiana.edu/~davidson/>.

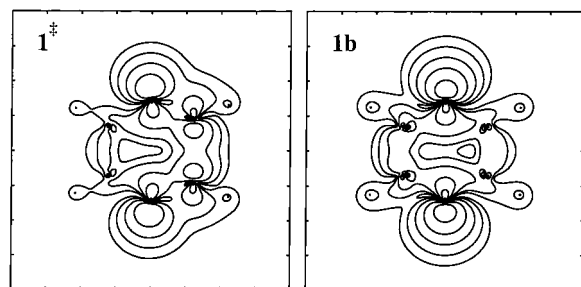


Figure 2. Contour plots of the in-plane density of effectively unpaired electrons for **1*** (left panel) and **1b** (right panel) calculated from the 10 $e^-/10$ orbital CASSCF/6-31G* wave function. The outermost contour is 0.001 $e/\text{\AA}^3$. Densities of consecutive levels differ by a factor of $\sqrt{10}$. Tick marks are 1 \AA apart.

Table 2. Number of Effectively Unpaired Electrons from the CASSCF Wave Functions for the 1^1A_1 , 1^3B_2 , and 2^1A States

atom	1a	1*	1b
1^1A			
C1,C6	0.26	0.19	0.29
C2,C5	0.23	0.53	0.94
C3,C4	0.18	0.38	0.19
1^3B			
C1,C6	0.43	0.72	0.19
C2,C5	0.25	0.63	0.23
C3,C4	0.80	0.51	1.10
2^1A			
C1	0.62		0.67
C2	0.82		0.47
C3	0.13		0.19
C4	0.71		0.23
C5	0.25		1.11
C6	0.41		0.18

lengths r_{32} , r_{34} , and r_{21} are within 0.005 \AA of experimental values.²⁷ Although the CASSCF nonbonded distance r_{16} agrees with the r_{16} values from comparable calculations employing larger basis sets, it is still 0.168 \AA larger than the experimental r_{16} . This deviation may be attributed to the dependence of r_{16} upon the bond angles α_{21H} , α_{321} , and α_{432} , that exceed the experimental angles by 0.8°, 1.4°, and 1.3°, respectively.

All methods predict a C_{2v} TS geometry that strongly resembles the diradical intermediate. The partially bonded carbons C1 and C6 are 1.92–2.12 \AA apart. The CASSCF TS wave function also has pronounced diradical character. The two configurations with the largest weights (the square of the coefficients in the CI expansion) in the wave function of **1***, $|\dots 8b_2^2\rangle$ (72%) and $|\dots 10a_1^2\rangle$ (10%), contribute 33 and 43%, respectively, to the wave function of **1b**. The $10a_1$ orbital is through-space bonding with respect to C2 and C5 while $8b_2$ is antibonding. Nevertheless, $8b_2$ has a lower orbital energy in **1b** because of through-bond interactions. Equal occupation would be expected for a diradical wave function in the absence of any interactions.

The similarity between the wave functions of **1*** and **1b** is also seen in the contour plots of the density of effectively unpaired electrons $D(\mathbf{r})$ (Figure 2, Table 2). Along the reaction coordinate, the total number of effectively unpaired electrons N_D (defined as the integral of $D(\mathbf{r})$ over the entire space) increases from 1.33 at the enediyne reactant, to 2.21 at the transition state, and reaches 2.97 at the diradical intermediate.²⁸ When a CASMP2 calculation is performed, the additional

Table 3. Thermodynamic Parameters (kcal/mol) for the Thermally Induced Bergman Cyclization of **1a** Computed with Various Methods and the 6-31G* Basis Set (ZPE and Thermal Corrections Included)

method	ΔG^\ddagger	ΔH^\ddagger	$T\Delta S^\ddagger$	ΔG_{rxn}	ΔH_{rxn}	$\Delta H_{\text{rxn}}^{\text{corr}}$	$T\Delta S_{\text{rxn}}$
expt ^b		28			8 \pm 3		
expt ^c		32			14		
CASMP2	26.86	24.22	-2.63	-1.83	-4.92		-3.08
CASSCF	44.18	41.86	-2.69	29.15	25.92		-3.23
UB3LYP	31.76	29.86	-1.90	6.51	3.94	3.64	-2.57
UBPW91	24.16	22.22	-1.94	3.43	0.71	-2.67	-2.71

^a Corrected for spin contamination with the sum formula. ^b See ref 39. ^c See ref 8.

electron correlation alters the TS such that the weight of the $|\dots 8b_2^2\rangle$ configuration increases from 72 to 88%, approaching the wave function of the enediyne in which this configuration contributes 93% to the total wave function. In agreement with previous reports, this shows that CASSCF overestimates the radical contribution to the TS wave function.²⁹

The singlet diradical intermediate **1b** has a distorted benzene geometry of D_{2h} symmetry, similar to previous studies.^{30,31} In particular, the C–C distances r_{34} and r_{16} (where both carbons are bonded to H atoms) are longer than r_{21} , r_{32} , r_{56} , and r_{45} (where one of the carbons is a radical center). The CASSCF prediction that $r_{16} < r_{34}$ (1.412 vs 1.442 \AA) is an artifact of the calculation, since the C1–C6 σ electrons are correlated and the C3–C4 σ electrons are not. In a delocalized MO picture (using the C_{2v} symmetry convention of **1a**), the occupied $8b_2$ orbital has some antibonding character from the σ^* orbital of the side bonds. Interestingly, in the CASSCF wave function, the $|\dots 8b_2^2\rangle$ configuration contributes slightly more than the $|\dots 8b_2^2\rangle$ configuration (43 vs 33%). The relative weights of these configurations is reversed in the CASMP2 wave function such that $|\dots 8b_2^2\rangle$ contributes 78% and $|\dots 10a_1^2\rangle$ only 17%.

Thermodynamic Description. DFT and CASSCF enthalpy differences are reported in Table 3. The UB3LYP ΔH^\ddagger and ΔH_{rxn} fall within the experimental margins of error, while UBPW91 performs less satisfactorily. This situation is reversed in RB3LYP and RBPW91 calculations, illustrating that restricted and unrestricted results do not necessarily parallel one another. In the analysis of the DFT results, the sum formula²² was used to correct the energy of the lowest-energy singlet diradical for triplet spin contamination.

The CASSCF ΔH^\ddagger (41.9 kcal/mol) and ΔH_{rxn} (25.9 kcal/mol) are significantly larger than either set of experimental values: 32 (or 28) and 14 kcal/mol (or 8 \pm 3), respectively.^{8,32} The theoretical ΔH^\ddagger is large because CASSCF overestimates the radical contribution to the TS wave function and underestimates the ion pair contribution,^{34,35} thereby elevating the TS energy. An MP2 calculation with the 8 $e^-/8$ orbital CASSCF reference wave function predicts that $H^\ddagger = 24.2$ kcal/mol.³³ For the same reason, $\Delta H_{\text{rxn}}^{\text{CASSCF}}$ is much larger than $\Delta H_{\text{rxn}}^{\text{CASMP2}}$. In CASMP2, the additional electron correlation for the ionic contributors to the diradical wave function leads to an exothermic value of $\Delta H_{\text{rxn}} = -4.9$ kcal/mol.

(29) Kraka, E.; Cremer, D. *J. Am. Chem. Soc.* **1994**, *116*, 4929.

(30) Lindh, R.; Lee, T. J.; Bernhardsson, A.; Persson, B. J.; Karlstrom, G. *J. Am. Chem. Soc.* **1995**, *117*, 7186.

(31) Borden, W. T.; Nicolaidis, A. *J. Am. Chem. Soc.* **1993**, *115*, 11951.

(32) Squires, R. R.; Nash, J. J.; Wierschke, S. G. *J. Am. Chem. Soc.* **1993**, *115*, 11958.

(33) The 8 $e^-/8$ orbital CAS was generated from the 10 $e^-/10$ orbital CAS by excluding the $1b_1$ and $3a_2$ MOs in **1a** and **1***, and the $1a_1$ and $2b_2$ MOs in **1b**.

(34) Davidson, E. R.; Borden, W. T. *Acc. Chem. Res.* **1996**, *29*, 67.

(35) Davidson, E. R. *J. Phys. Chem.* **1996**, *100*, 6161.

(27) McMahon, R. J.; Halter, R. J.; Fimmen, R. L.; Wilson, R. J.; Peebles, S. A.; Kuczkowski, R. L.; Stanton, J. F. *J. Am. Chem. Soc.* **2000**, *122*, 939.

(28) 0.27 unpaired electrons per π bond is typical.

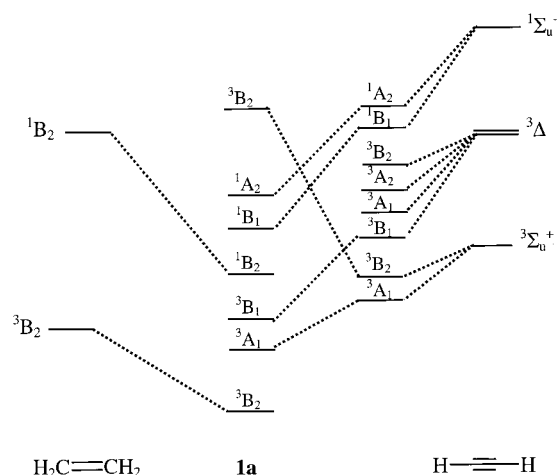


Figure 3. The MO correlation diagram for the formation of **1a** from ethylene and acetylene.

Table 4. Vertical Excitation Energies (in eV) of the First Six Excited States of **1a** Computed with CI, CASSCF, and CASMP2 Methods

method	3B_2	3A_1	3B_1	1B_2	1B_1	1A_2
CI	3.900	7.258	6.536	8.175	7.833	8.056
CASSCF	3.419	6.183	6.385	7.102	6.794	^b
CASMP2a	3.120	4.998	5.103	5.598	5.725	5.806

^a Mixed orbitals from roots 2–4 were used to achieve SCF convergence. ^b Not converged with pure state orbitals.

Excited States of the Enediyne Moiety

The Weakly-Interacting Ethylene Acetylene Model. In the simplest description, excited states of **1a** may be regarded as linear combinations of the configurations of one ethylene unit and two acetylene units. The ethylene unit contributes one ($\pi_{\perp}, \pi_{\perp}^*$) excited configuration of B_2 symmetry. Each acetylene unit can contribute $^1,^3\Delta$ and $^1,^3\Sigma^{\pm}$ states which can be combined to form 16 excited configurations. In this case, only the lowest-energy configurations derived from $^3\Sigma$, $^3\Delta$, and $^1\Sigma$ need be considered. When classified in C_{2v} symmetry, these are the ($\pi_{\perp}, \pi_{\perp}^*$) and ($\pi_{||}, \pi_{||}^*$) configurations of A_1 and B_2 symmetry, respectively, and the ($\pi_{\perp}, \pi_{||}^*$) and ($\pi_{||}, \pi_{\perp}^*$) configurations of A_2 and B_1 symmetry, respectively. When electron repulsion is introduced to this model, the interaction of the acetylene units with each other and the ethylene motif lifts the degeneracy of the acetylene excitations and leads to a broad energetic distribution of enediyne excited states (Figure 3).

The first three singlet and triplet vertical excited states of **1a** have been examined by CASCI, CASSCF, and CASMP2 methods. The CASCI calculations were performed with the CASSCF orbitals of S_0 as the initial guess. Because the excited-state MOs are not optimized in the CASCI method, they provide a poor description of the excited-state wave function. Among the three methods, CASCI produces the highest vertical excitation energies (ΔE) from S_0 (Table 4). Optimization of the excited-state MOs in the CASSCF calculation lowers ΔE by an average of 1 eV (23 kcal/mol). Interestingly, the excitation energies are further lowered in the CASMP2 description with the 8 e^- /8 orbital CASSCF reference wave function. Contrary to intuition, the CASMP2 calculation recovers more correlation energy for the excited state than for the ground state. The CASMP2 excitation energies are treated here as the most reliable.

Triplet States. All three methods predict that the spectroscopically forbidden 1B_2 ($|\dots 2b_1^1 2a_2^1\rangle$), 1B_1 ($|\dots 8b_2^1 2a_2^1\rangle$), and

1A_1 ($|\dots 1a_2^1 2a_2^1\rangle$) triplet states lie between the singlet ground state (S_0) and the first singlet excited state. The relative energy ordering of 1B_2 and 1B_1 states depends on the method of the calculation (Table 4). The 1B_2 state ($\pi_{\perp}, \pi_{\perp}^*$) is 3.12 eV above S_0 . The vertical singlet–triplet gap $\Delta E_{ST}(^1B_2, ^1B_2)$ is 2.5 eV. This is significantly larger than the singlet–triplet gap of any other pair of states, making the 1B_2 state of the enediyne isolated by energy and symmetry. Since the 1B_2 state of the enediyne is very similar to the 1B_2 state of ethylene, the vertical $\Delta E_{ST}(^1B_2, ^1B_2)$ in the enediyne remains relatively close to that of ethylene (2.5 vs 3.4 eV³⁶).

The states 1A_1 ($\pi_{\perp}, \pi_{\perp}^*$) and 1B_1 ($\pi_{||}, \pi_{\perp}^*$) are nearly degenerate, lying 5.00 and 5.10 eV above S_0 , respectively. Both states are derived from acetylene configurations and are therefore localized at the alkyne units.

Singlet States. In the CASMP2 description, the three lowest-energy singlet excited states appear in the following order: 1B_2 ($\pi_{\perp}, \pi_{\perp}^*$) ($|\dots 2b_1^1 2a_2^1\rangle$), 1B_1 ($\pi_{||}, \pi_{\perp}^*$) ($|\dots 8b_2^1 2a_2^1\rangle$), and 1A_2 ($\pi_{||}, \pi_{\perp}^*$) ($|\dots 9a_1^1 2a_2^1\rangle$). CASSCF, however, predicts the reverse order of the 1B_2 and 1B_1 states. The $S_0 \rightarrow ^1B_2$ transition is strongly absorbing, while the $S_0 \rightarrow ^1B_1$ is weakly absorbing and the $S_0 \rightarrow ^1A_2$ is symmetry forbidden. Like their triplet counterparts, the 1B_2 state is localized at the ethylene unit, while the 1B_1 and 1A_2 states are localized at the alkyne units.

Applications of the Model. The weakly interacting ethylene–acetylene model is supported by experiment. For example, our model predicts that symmetric substitution at the alkyne termini will not affect $\Delta E_{ST}(^1B_2, ^1B_2)$ of the enediyne because both 1B_2 and 1B_2 are derived from ethylene. Indeed *n*-propyl- and phenyl-substituted enediynes have the same experimentally observed energy difference between the fluorescent and phosphorescent states (predicted by CASSCF to be the adiabatic 1B_2 and 3B_2 states, respectively).¹⁰ Other predictions are possible regarding the energetic distribution of enediyne excited states. First, it appears that the degree of stabilization of the 3B_2 state of the enediyne is related to the magnitude of $\Delta E_{ST}(^1B_2, ^1B_2)$ of ethylene. The energy of both the vertical and adiabatic 3B_2 states of the enediyne should increase upon substitution of the ethylene unit with a fragment whose corresponding ΔE_{ST} is smaller than in ethylene. Conversely, the energy of the 3B_2 state is expected to decrease upon substitution with a fragment whose analogous ΔE_{ST} is larger than in ethylene. The available phosphorescence data shows that the increase in phosphorescence energy [adiabatic $\Delta E_{ST}(S_0, ^3B_2)$] from 2.1 eV in **1a** (by CASMP2) to 2.4–2.9 eV¹⁰ in (*Z*)-3,4-benzo-1,6-*n*-propyl-hex-3-ene-1,5-diyne and (*Z*)-3,4-benzo-1,6-phenyl-hex-3-ene-1,5-diyne is paralleled by the decrease in the $\Delta E_{ST}(^1B_2, ^1B_2)$ that occurs when the ethylene unit [$\Delta E_{ST}(^1B_2, ^1B_2) \approx 3.4$ eV] is replaced by a benzene ring [$\Delta E_{ST}(^1B_2, ^1B_2) \approx 2$ eV³⁷]. Second, the states of the enediyne that are produced by excitations in the acetylene moiety can be manipulated by varying substituents at the alkyne termini or by introducing geometric distortions that increase the interaction between the acetylene fragments. Either of these perturbations would alter ΔE_{ST} of the ($\pi_{||}, \pi_{\perp}^*$) and ($\pi_{||}, \pi_{||}^*$) configurations and thereby change the energy of the respective states.

Lowest-Energy Triplet PES

Geometry and Electronic Structure. Assuming the preservation of C_{2v} molecular symmetry, Bergman cyclization along

(36) Peyerimhoff, S. D.; Buenker, R. J. *Theor. Chim. Acta* **1972**, 27, 243.

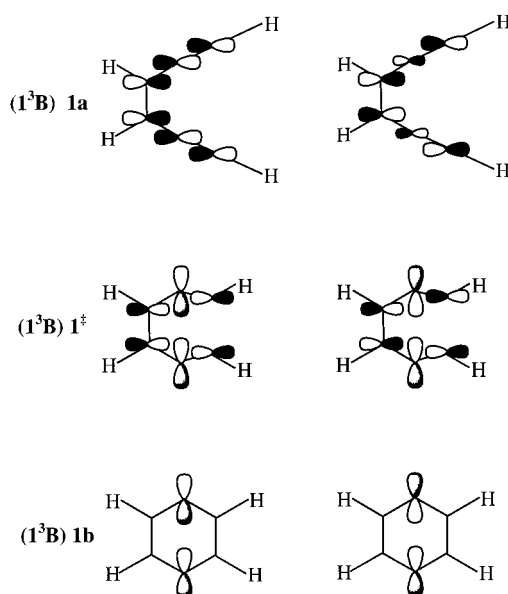
(37) Lim, E. C., Ed. *Excited States*; Academic Press: New York, 1982; Vol. 5, pp 57–74.

Table 5. ^{13}B Excited-State Structures of **1a**, **1[†]**, and **1b** Computed with Various Methods

system	method	r_{25}	r_{16}	r_{32}	r_{34}	r_{21}	$\alpha_{21\text{H}}$	α_{321}	α_{432}	ω_{2345}
1a	CASSCF	3.439	5.361	1.403	1.479	1.221	179.3	179.5	122.2	93.16
	UB3LYP	3.401	5.329	1.376	1.482	1.227	179.4	179.9	122.5	92.31
	UBPW91	3.411	5.365	1.378	1.485	1.239	179.2	179.6	122.5	93.19
1[†]	CASSCF	2.779	2.150	1.383	1.461	1.295	139.9	136.6	117.1	26.05
	UB3LYP	2.730	2.192	1.361	1.496	1.286	144.5	139.4	115.4	28.69
	UBPW91	2.759	2.275	1.367	1.501	1.285	145.4	140.3	115.7	29.58
1b	CASSCF	2.683	1.425	1.385	1.405	1.387	121.4	125.6	117.5	0.0
	UB3LYP	2.647	1.409	1.381	1.409	1.381	122.3	126.7	116.6	0.0
	UBPW91	2.655	1.417	1.387	1.417	1.387	122.4	127.0	116.5	0.0

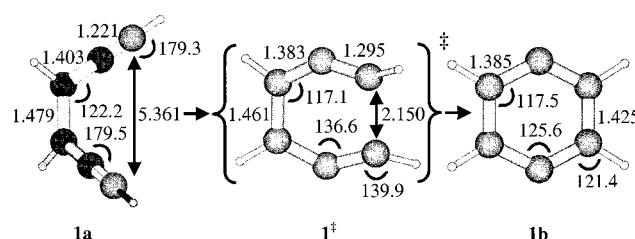
Table 6. UDFT and CASSCF Mulliken Spin Populations for **1a**, **1[†]**, and **1b** in the ^{13}B State

	1a			1[†]			1b		
	UB3LYP	UBPW91	CASSCF	UB3LYP	UBPW91	CASSCF	UB3LYP	UBPW91	CASSCF
C1	0.578	0.572	0.322	0.492	0.514	0.391	−0.008	−0.014	0.007
C2	−0.278	−0.239	−0.135	0.049	0.024	0.206	0.962	0.967	0.984
C3	0.736	0.700	0.802	0.464	0.471	0.390	−0.008	−0.014	−0.005
C4	0.736	0.700	0.802	0.463	0.470	0.390	−0.008	−0.014	−0.005
C5	−0.278	−0.239	−0.135	0.049	0.024	0.206	0.962	0.967	0.984
C6	0.578	0.572	0.322	0.492	0.514	0.391	−0.008	−0.014	0.007

**Figure 4.** Singly occupied molecular orbitals ($10b_1$, $11a_1$) of the lowest-energy triplet (^{13}B) states of **1a**, **1[†]**, and **1b** (out-of-plane orbitals represented in black, in-plane orbitals represented in gray).

the lowest-energy triplet PES is a Woodward–Hoffmann forbidden process because the $^{13}\text{B}_2$ state of **1a** is dominated by a $(\pi_{\perp}, \pi_{\perp}^*)$ excited configuration, while the corresponding state of **1b** is primarily $(\pi_{\parallel}, \pi_{\parallel}^*)$ (Figure 4). Although the triplet enediyne and diradical can both be adequately described by single determinants, the wave function of **1[†]** must include the configurations of both species. Mixing between the out-of-plane and in-plane configurations is only possible in species with a lower symmetry. Thus, the reaction becomes allowed in C_2 symmetry. At the same time, the geometric distortion that is responsible for lowering molecular symmetry may also result in competitive reaction pathways.

As in ethylene itself, DFT and CASSCF methods predict that rotation about the ethylene bond causes the vertical $^{13}\text{B}_2$ state of **1a** to relax to the adiabatic ^{13}B state of C_2 symmetry (Table 5, Figure 5). The distortion is possible because of the single-electron occupation of the bonding ($p_{3\perp} + p_{4\perp}$) and antibonding ($p_{3\perp} - p_{4\perp}$) atomic orbital combinations of the $10b$ and $11a$ MOs (the $2b_1$ and $2a_2$ MOs in C_{2v} symmetry) (Figure 5).

**Figure 5.** $10\text{ e}^-/10\text{ orbital}$ CASSCF/6-31G* optimized structures along the lowest-energy triplet PES for the Bergman cyclization of **1a**.

Interestingly, UBPW91 and CASSCF produce similar structures that are somewhat different from UB3LYP. The dihedral angle ω_{2345} , measuring the rotation about the C3–C4 axis, is predicted to be $92\text{--}93^\circ$ by each method. The slightly obtuse ω_{2345} allows partial π bonding between C3–C4 so that the distance r_{34} is shorter than the ordinary C–C bond length of 1.54 \AA . The major effect of twisting about the C3–C4 axis is an increase in the distance r_{16} averaging roughly 0.9 \AA in the three methods. This distortion increases the probability of a competing cis–trans isomerization pathway. Although the products of this path have been observed experimentally,¹² isomerization can be prevented by manipulating substituents at C3 and C4.

When isomerization is suppressed, the unpaired electron density comes to play an important role in enediyne reactivity. Analysis of Mulliken spin population and $D(\mathbf{r})$ ³⁸ predicts that the unpaired electron density is localized in the p_{\perp} AOs of the ethylene and terminal alkyne carbons (Table 6, Table 2, Figure 6). Because the C_2 structure of **1a** is nonplanar, we plotted $D(\mathbf{r})$ for the vertical excited $^{13}\text{B}_2$ state of C_{2v} symmetry (Figure 6). This should be a reasonable approximation to the density $D(\mathbf{r})$ in the distorted ^{13}B geometry because the total number of effectively unpaired electrons changes insignificantly upon relaxation from the planar vertical state to the nonplanar adiabatic state (3.04 at the C_{2v} vs 2.98 at the C_2).

The C1 and C6 radical centers may participate in premature H-atom abstraction rather than Bergman cyclization. One may expect that H-atom abstraction by one of the terminal alkyne carbons (C1 or C6) will greatly increase the radical character of the adjacent carbon (C2 or C5). This is confirmed by the

(38) Unlike spin density, $\rho_{\mu}(\mathbf{r}) = \rho_{\alpha}(\mathbf{r}) - \rho_{\beta}(\mathbf{r})$, the density $D(\mathbf{r})$ is always nonnegative.

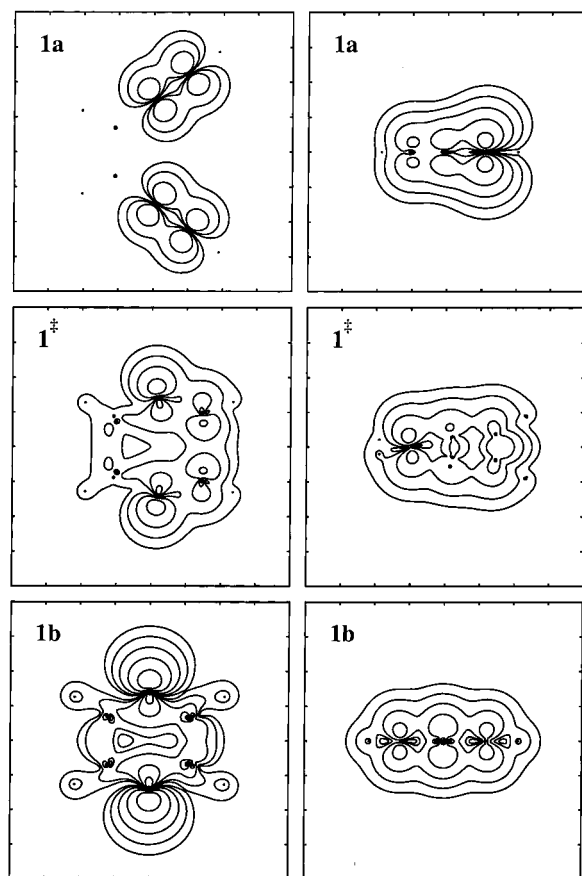


Figure 6. Contour plots of the density of effectively unpaired electrons for the lowest-energy vertical triplet state of **1a** and the adiabatic triplet states of **1*** and **1b** computed from the CASSCF/6-31G* wave functions. (**1a** left panel: in-plane section, right panel: out-of-plane morphed density. **1*** left panel: in-plane morphed density, right panel: out-of-plane morphed density. **1b** left panel: in-plane section, right panel: out-of-plane morphed density.)

calculation of the spin populations and density $D(\mathbf{r})$ in several systems (Figure 7). The products of abstraction proceed to react in some fashion at the radical center. These results agree with the experimentally reported photoreduction products that are produced upon photosensitization of aromatically substituted enediyne (where the cis-trans isomerization pathway has been prevented by replacing the ethylene unit with a benzene ring).¹⁰

Because of the possibility of competitive reactions, it is unlikely that population of the 1^3B state of **1a** will lead to Bergman cyclized products. However, if the competing isomerization and H-atom abstraction pathways could be inhibited, then cyclization becomes possible. Along the 1^3B PES for the Bergman cyclization of **1a**, DFT predicts nearly the same early TS of C_2 symmetry as the CASSCF method (Table 4, Figure 5). The dihedral angle ω_{2345} is 26–29°. The CASSCF wave function is dominated by a single $|\dots 10b^1 11a^1\rangle$ configuration (70%) whose two singly occupied orbitals contain the out-of-plane excitation of the triplet enediyne and the in-plane excitation of the diradical (Figure 4). Since this configuration is the only one present in DFT, the single determinant description is similar to the multideterminant one.

Although there are many similarities between the DFT and CASSCF descriptions of the triplet TS, there are some important differences. DFT predicts that the excess spin at the TS is localized at C1, C3, C4, and C6 and that the atomic spin populations of C2 and C5 increase from 0.28 in **1a** to nearly zero (Table 6). This indicates that the DFT “wave function” is

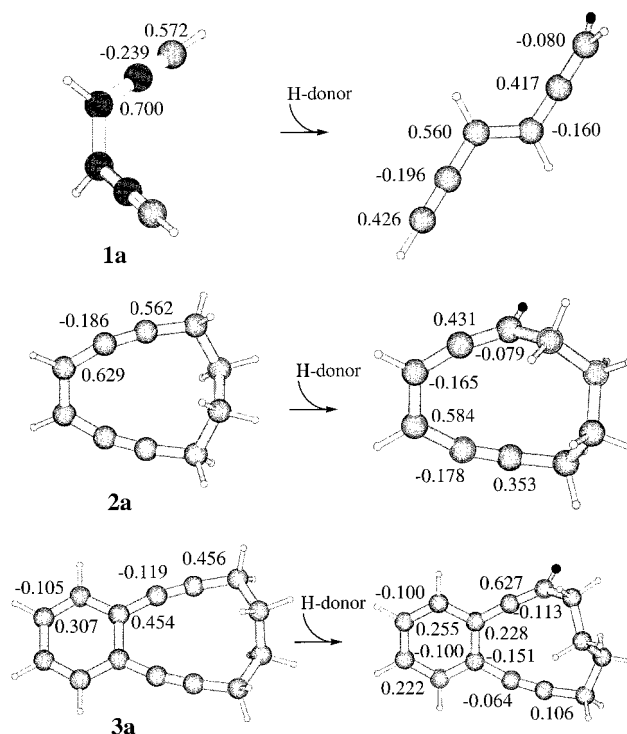


Figure 7. UBPW91/6-31G* Mulliken atomic spin populations at the optimum geometry of the $3B$ states of **1a**, **2a**, and **3a** and the corresponding dienynes resulting from H atom abstraction at the alkyne carbon.

Table 7. Thermodynamic Parameters of the Bergman Cyclization of **1a–3a** along the Lowest-Triplet PES (1^3B) Calculated with Various Methods (ZPE and Thermal Corrections Included)

system	method	ΔG^\ddagger	ΔH^\ddagger	$T\Delta S^\ddagger$	ΔG_{rxn}	ΔH_{rxn}	$T\Delta S_{\text{rxn}}$
1a	CASMP2	24.31	21.42	-2.89	-37.80	-41.80	-4.00
	CASSCF	40.81	37.57	-3.24	-18.13	-22.55	-4.42
	UB3LYP	29.27	27.65	-2.26	-33.49	-37.22	-3.73
2a	UBPW91	24.27	21.35	-2.67	-35.24	-39.32	-4.08
	UB3LYP	17.75	15.61	-2.13	-38.48	-41.32	-2.84
3a	UBPW91	11.90	9.53	-2.37	-39.55	-42.75	-3.20
	UB3LYP	15.16	13.15	-2.01	-43.57	-46.72	-3.15
	UBPW91	10.00	7.79	-2.21	-43.32	-46.70	-3.38

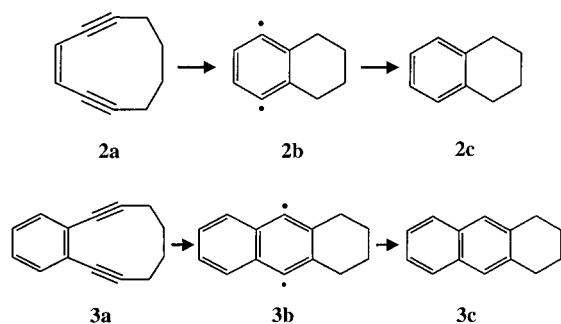
closer to the excited enediyne than to the triplet diradical. In the CASSCF TS the unpaired electron density is essentially delocalized (Figure 6, Table 2). This difference between the DFT and the CASSCF descriptions arises from the several excited electronic configurations that make up 30% of the CASSCF wave function but are absent in DFT.

As the reaction proceeds from the TS to the triplet diradical intermediate, the symmetry increases from C_2 to D_{2h} . The geometry of the triplet diradical **1b** is less distorted than its S_0 counterpart. Both DFT and CASSCF methods predict shortening of the r_{16} and r_{34} bond distances and lengthening of r_{21} , r_{32} , r_{56} , and r_{45} . These geometric differences may be attributed to the decreased electron occupation of the $10b_1$ MO which is partially delocalized into the σ^* orbitals of the C1–C6 and C3–C4 bonds (where the C_2 symmetry notation of triplet **1a** is used).

Thermodynamic Description. Thermochemical parameters of the Bergman cyclization of **1a** along the lowest-energy triplet PES are presented in Table 7. DFT methods predict ΔG^\ddagger , ΔH^\ddagger , and $T\Delta S^\ddagger$ values similar to those for the S_0 reaction. This is somewhat surprising given the large structural rearrangement that is necessary to form the triplet TS. Consequently, we calculated the triplet cyclization PES for two other systems, (Z)-

Table 8. 2^1A Excited-State Structures (r in Å, α in Degrees) of **1a** and **1b**

system	r_{21}	r_{16}	r_{25}	r_{32}	r_{34}	r_{45}	r_{56}	α_{21H}	α_{321}	α_{432}	α_{456}
1a	1.367	4.444	2.995	1.330	1.448	1.405	1.219	113.8	168.1	125.4	180.7
1b	1.456	1.458	2.873	1.456	1.372	1.432	1.346	118.0	112.0	124.1	124.7

Scheme 2

cyclodec-3-ene-1,5-diyne (**2a**) and 3,4-benzocyclodec-3-ene-1,5-diyne (**3a**) that undergo less geometric distortion in the 1^3B state than **1a** (Scheme 2).

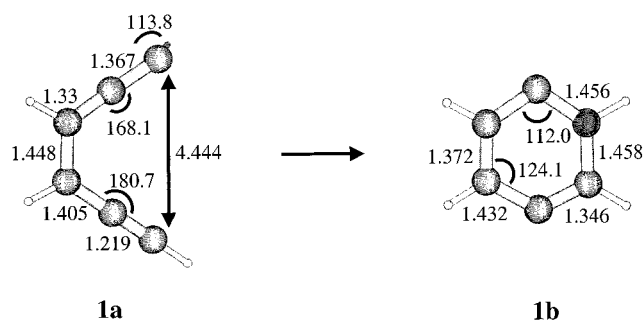
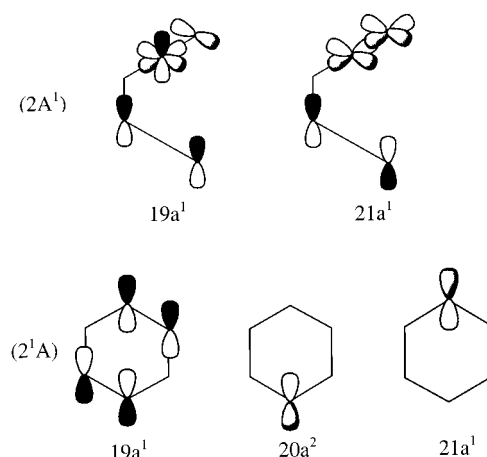
The adiabatic singlet–triplet gap $\Delta E_{ST}(S_0, 1^3B)$ was found to be inversely proportional to the degree of distortion of the 1^3B state. Compound **1a**, which undergoes the largest distortion, has the most stabilized 1^3B state ($\Delta E_{ST}^{UB3LYP} = 44$ kcal/mol). Compound **2a**, which is less distorted than **1a** because the enediyne is part of a ten-membered ring, has $\Delta E_{ST}^{UB3LYP} = 47$ kcal/mol. Last, the most rigid molecule, **3a**, has the least stabilized 1^3B state ($\Delta E_{ST}^{UB3LYP} = 62$ kcal/mol). Table 8 shows that rotation about the C3–C4 bond stabilizes the triplet enediyne more than the triplet TS which leads to the observed values of ΔG^\ddagger , ΔH^\ddagger , and $T\Delta S^\ddagger$ for systems **1a**, **2a**, and **3a**. In all instances, DFT predicts that the cyclization is very exothermic and that the ΔG_{rxn} and ΔH_{rxn} occur within 10 kcal/mol between the three systems.

Because the absolute CASSCF energy of **1a** is much lower than the DFT value, the CASSCF description of the triplet PES involves a higher activation barrier and a less exothermic pathway than the DFT description. CASMP2 calculations recover the most electron correlation energy in **1⁺** and **1b**, indicating that the corresponding CASSCF wave functions are insufficient for an accurate description.³⁸ However, MRSDCI wave functions do not contain significant configurations that lie outside of the active space of the CASSCF method. The poor CASSCF description of **1⁺** and **1b** can then be attributed to the cumulative effect of many excitations with small configuration coefficients that involve virtual orbitals outside of the active space.

First Excited Singlet PES

Geometry and Electronic Structure. The Bergman cyclization along the first excited singlet (S_1) PES, with the preservation of C_{2v} molecular symmetry is also Woodward–Hoffmann forbidden. CASSCF predicts that the first vertical singlet state of **1a** is 1^1B_1 ($\pi_{||}, \pi_{\perp}^*$), while the corresponding state of **1b** is 1^1A_1 ($\pi_{\perp}, \pi_{||}^*$).

The vertical 1^1B_1 state of **1a** relaxes through a second-order Jahn–Teller distortion to a 2^1A state of C_1 symmetry (Table 8, Figure 8). Intermixing between the 1^1B_1 and 1^1A_2 states (Figure 3) localizes the distortion at one alkyne unit (for the purposes of clarity assumed to be the C1–C2 unit) which elongates r_{21} from 1.208 to 1.367 Å, and constricts α_{21H} from 179.4° to 113.8°. The $|\dots 19a^1 21a^1\rangle$ configuration dominates both the

**Figure 8.** Singly occupied molecular orbitals of the first singlet excited states of **1a** and **1b** (out-of-plane orbitals represented in black, in-plane orbitals represented in gray).**Figure 9.** 10 e[−]/10 orbital CASSCF/6–31G* optimized structures along the first excited singlet (2^1A) PES for the Bergman cyclization of **1a**.

CASSCF and the CASMP2 wave functions. The singly occupied MOs are a mixture of p_{\perp} , $p_{||}$, and sp_{σ} AOs (Figure 9) which causes the two effectively unpaired electrons to be present in both the parallel and perpendicular planes of the molecule (Figure 10). In particular, the effectively unpaired electrons are localized in the p_{\perp} AO of C4, the p_{\perp} , $p_{2||}$ AOs and sp_{σ} hybrid AO of C2, and the $p_{||}$ AO and sp_{σ} hybrid AO of C1 (Table 2).

We believe that H-atom abstraction by C1 or C2 is unlikely because the unpaired electrons are not entirely confined to any single p AO. On the other hand, H-atom abstraction by C4 is possible but may be prevented by substitution at C3 and C4. Even if the reactivity of C4 is suppressed, two other reaction pathways from the 2^1A state of **1a** still remain: deactivation from the 2^1A state to S_0 and Bergman cyclization along the 2^1A PES. Either of the two paths will generate Bergman product.

On the 2^1A PES for Bergman cyclization, the geometry optimization of the TS has been plagued with convergence difficulties. A CASSCF linear synchronous transit (LST) calculation predicts that an energy maximum with only one imaginary vibration occurs when **1a** distorts such that $r_{56} = 1.34$ Å, $\alpha_{456} = 136.2^\circ$ and $\omega_{2345} = -0.5^\circ$. The corresponding wave function is dominated by a configuration corresponding to $(\pi_{||}, \pi_{\perp}^*)$ and $(\pi_{\perp}, \pi_{||}^*)$ excitations from S_0 which decreases the in-plane electron repulsion at the TS relative to the 1^1A_1 and 1^3B TS.

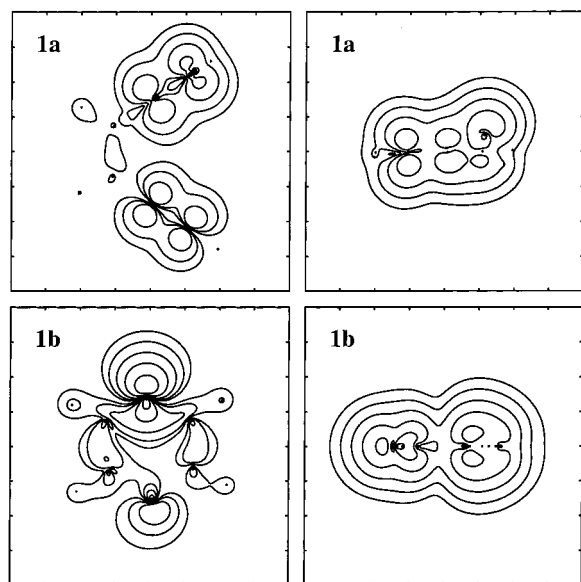


Figure 10. Contour plots of the density of effectively unpaired electrons for first singlet excited states of **1a**, and **1b** computed from the 10 $e^-/10$ orbital CASSCF/6-31G* wave functions (**1a** left panel: in-plane morphed density, right panel: out-of-plane morphed density. **1b** left panel: in-plane section, right panel: out-of-plane morphed density.)

Both the CASSCF and CASMP2 wave functions of the 2^1A state of **1b** are dominated by the $|\dots 19a^1 20a^2 21a^1\rangle$ configuration. The two singly occupied orbitals generate an open shell diradical that is localized at one of the dehydrocarbon centers, while the doubly occupied 20a MO is best described as a singlet carbene localized at the opposite carbon center (Figure 9, Figure 10). This unique electronic structure distorts **1b** to a C_1 geometry. Decreased occupation of the π bonding MO 19a increases the r_{32} , r_{21} , and r_{45} distances relative to the geometry of the 1^1A_1 state of **1b**. Interestingly, correlation of the C1–C6 σ electrons not only leads to $r_{16} > r_{34}$, but also may shorten r_{56} because the unpaired electron density at C6 delocalizes into the singly occupied 21a MO.

Thermochemical Parameters. Both CASSCF and CASMP2 methods predict that cyclization along the 2^1A PES is exother-

mic ($\Delta G_{\text{rxn}}^{\text{CASSCF}} = -1.31$ kcal/mol, $\Delta G_{\text{rxn}}^{\text{CASMP2}} = -14.82$ kcal/mol, $\Delta H_{\text{rxn}}^{\text{CASSCF}} = -5.55$ kcal/mol, $\Delta H_{\text{rxn}}^{\text{CASMP2}} = -18.39$ kcal/mol).⁴⁰ However, since the 2^1A state of **1b** is higher in energy than the 1^3B state of **1b**, the cyclization is less exothermic along the 2^1A PES than the 1^3B PES ($\Delta H_{\text{rxn}}^{\text{CASMP2}} = -42$ kcal/mol). Although the minimum energy of the TS was not obtained, the CASSCF LST calculation puts an upper bound on the TS energy such that $\Delta E^\ddagger \leq 32$ kcal/mol (ZPE not included). The upper bound to the 2^1A PES activation barrier is similar to that of the 1^1A and 1^2B PES for Bergman cyclization.

Conclusions

The weakly interacting ethylene-acetylene model offers a simple description of enediyne excited states. States that correspond to excitations of the ethylene fragment may either isomerize to the *trans*-1,5-hexadiyne-3-ene conformer, undergo H-atom abstraction at the terminal alkyne carbons, or Bergman cyclize to the 1,4-phenyl diradical. Of the three mechanisms induced by excitation of the ethylene fragment, Bergman cyclization is the least probable. In contrast, enediyne excited states that correspond to excitations of the acetylene fragments have a smaller number of competitive pathways and are expected to form Bergman product. Our conclusions are consistent with the experimental studies of the photochemical Bergman cyclization and may provide predictive insights into the design of more photochemically labile enediyne compounds.

Acknowledgment. We thank the Graduate Assistance in Areas of National Need (GAANN) program administered by the Department of Education for a teaching/research assistantship. This work was partially supported by Grant No. CHE-9982415 from the National Science Foundation and Grant No. RPG-99-156-01-C from the American Cancer Society.

JA0039987

(39) The 8 $e^-/8$ orbital CAS was generated from the 10 $e^-/10$ orbital CAS by excluding the 1a and 5a orbitals in **1a** and **1**⁺, and the 1a and 5a orbitals in **1b**.

(40) The 8 $e^-/8$ orbital CAS was generated from the 10 $e^-/10$ orbital CAS by excluding the 16a and 25a orbitals in **1a** and **1b**.

(41) Squires, R. R.; Wenthold, P. G. *J. Am. Chem. Soc.* **1994**, *116*, 6401.